



Research article

Performance evaluation of nanofluid-based photovoltaic thermal (PVT) system with regression analysis

A.K. Azad^{a,b,*}, Salma Parvin^b, Tahiya Hossain^c^a Department of Natural Sciences, Islamic University of Technology (IUT), Gazipur, 1704, Bangladesh^b Department of Mathematics, Bangladesh University of Engineering and Technology (BUET), Dhaka, 1000, Bangladesh^c Department of Mechanical and Production Engineering, Islamic University of Technology (IUT), Gazipur, 1704, Bangladesh

ARTICLE INFO

Keywords:

Photovoltaic thermal
Performance analysis
Reynolds number
Regression analysis
Solar irradiation
Month effect
Carbon nanotube nanofluid

ABSTRACT

The recent global energy crisis has shocked Bangladesh's power sectors, and experts recommend using alternative energy sources to conserve natural gas, fossil fuels, and electricity. Numerous investigations on the photovoltaic thermal (PVT) system have been carried out to get the source efficiently. As a result, a parametric evaluation of the PVT system's efficiency in Dhaka, Bangladesh, is investigated numerically using CNT nanofluid as a coolant. The numerical simulation is performed using the Galerkin weighted residual based finite element method. For accurate computations, the meteorological data for Dhaka, Bangladesh, is taken from open sources of Renewables.ninja. The effect of regulating parameters Reynolds number ($200 \leq Re \leq 1000$), solar irradiation ($200 \text{ W/m}^2 \leq G \leq 1000 \text{ W/m}^2$), and the monthly influence on performance such as cell temperature, fluid domain exit temperature, efficiencies, and energy are discussed. In addition, regression analyses of electrical efficiency and thermal efficiency are discussed for the input variables Reynolds number and solar irradiation. After postprocessing, empirical results are compiled and presented as 3D surface graphs, tables, and line diagrams. As the Reynolds number increased, the cell temperature and discharge temperature decreased, resulting in increased efficiency. However, the opposite situation is found for solar irradiation. Month-to-month variation also has a considerable impact on photovoltaic thermal performance. This research will help to improve the efficacy of PVTs in Dhaka, Bangladesh, by identifying useful alternative renewable energy sources.

1. Introduction

In recent times, Bangladeshi people have been facing frequent power interruptions. Due to rising global energy prices, Bangladesh has been forced to limit its power output and increase its reliance on imported fossil fuels like Liquefied Natural Gas (LNG). As a result of Bangladesh's ongoing power crisis — caused by a gas shortage — experts advise the Bangladeshi government to take the initiative to gradually switch to renewable energy sources for instance, solar energy. The International Energy Agency (IEA) report states that about two-thirds of the plant capacity installed in 2016 came from renewable sources. Additionally, photovoltaics (PV) expanded more quickly than other sources in 2016, while the capacity of other renewable sources only increased by 4%. The entire PV capacity worldwide is anticipated to increase to 740 GW by 2022 [1]. Thus, research aimed at increasing PV cell efficiency is of the utmost

* Corresponding author. Department of Natural Sciences, Islamic University of Technology (IUT), Gazipur, 1704, Bangladesh.
E-mail address: azad@iut-dhaka.edu (A.K. Azad).

significance. According to studies, each degree of temperature increase reduces PV efficiency by 0.4% [2]. As a result, many hybrid systems of active and passive PV cooling solutions have been designed in the past [3–6].

Hybrid photovoltaic thermal (PVT) systems effectively harness solar energy [7] from combined photovoltaic and thermal systems. This system produces high-quality electricity from photovoltaic PV panels and heat from heat transfer fluid (HTF) attached at the back of PV panels through cogeneration utilizing the thermal power of the PV panels. Thus, the efficiency of a solar PV panel rises by around 20% [8]. Nahar et al. [9] analyzed PVT performance in Malaysia without an intermediate absorber plate using numerical and experimental studies. They carried out a 3D numerical analysis with the COMSOL Multiphysics program, which uses the finite element method (FEM). They used their outdoor experimental studies to validate their numerical results. The combined performance of the PVT system at 1000 W/m^2 of irradiance and $34 \text{ }^\circ\text{C}$ inlet and ambient temperatures were calculated to be 84.4% numerically and 80% experimentally. They also suggested that the established simulation model may be applied to other thermal collector designs utilizing different materials. Yildirim et al. [10] examined the electrical and thermal efficiency of a PVT system with a 325 W PV panel using the energy balance method. To achieve optimal cooling, they evaluated different inflow velocities and temperatures. Additionally, the performance of PV and PVT modules was assessed. Their research indicates that the electrical efficiency of PV at a mass flow rate of 0.014 kg/s and an inlet flow temperature of $15 \text{ }^\circ\text{C}$ is 17.79% and the thermal efficiency is 76.13%. Gomaa et al. [11] thoroughly analyzed two unique design techniques (micro and large thickness layout) on a hybrid PVT for a cross-fined channel box with varying coolant mass flows and irradiance. Using ANSYS software, a three-dimensional finite element-based numerical simulation was conducted. The ideal cooling fluid flow rate was found to be 3 l/min for both thin and thick box heat exchangers.

The limitations of conventional HTFs include their poor thermophysical properties and the absence of application-specific parameter tuning. Nanofluids have been discovered to have superior thermal, optical, and heat transport capabilities in compared to the many traditional HTFs [12–16]. By numerical and experimental analyses, PVT systems using MWCNT-based water nanofluid were studied for their energy and exergy efficiency by Fayaz et al. [17]. They utilized the FEM-based COMSOL Multiphysics tool to solve their model numerically, validate it with their experimental results, and then evaluate and contrast the efficiency of their new PVT system with that of other established PVT systems. They observed that employing MWCNT nanofluid as a cooling fluid instead of water resulted in 4% higher PV cell efficiency for numerical simulation and 3.67% for experimental testing. Additionally, the overall efficiency for the experimental study was 87.67%, and the numerical study was 89.2% at solar irradiation, $R = 1000 \text{ W/m}^2$. Murtadha and Hussein [18] experimented with the efficacy of a monocrystalline-based PVT system employing an Al_2O_3 /water nanofluid with varying flow velocity. Panel electrical efficiency is increased by 20.2% for turbulent flow and 15% for laminar flow when using a 3% Al_2O_3 /water nanofluid instead of a regular PV panel. Diwania et al. [19] assessed the thermal and electrical efficiency of a serpentine tube-based PVT setup through research in Ghaziabad, India, using nanofluids of Cu-water and TiO_2 -water. As a cooling fluid, it was observed that the Cu/water nanofluid performed better than the TiO_2 /water nanofluid. Specifically, at a volume concentration of 1%, the Cu/water nanofluid demonstrated a temperature reduction of $4.1 \text{ }^\circ\text{C}$, resulting in an increase in electrical efficacy of 5.98% compared to using water alone as the cooling fluid. Recently, in another study, Diwania et al. [20] assessed the efficacy of a PVT system utilizing Fe/water nanofluid and day-ahead forecasting input data in Roorkee, India, using a machine learning process. Compared to a water-cooled PVT system, the hPVT collector's total efficiency was 9.84% higher when a 2% Fe/water nanofluid was used. Finally, the results demonstrate that the predicted data closely match the actual data. Recent research by Diniz et al. [21] utilized plasmonic nanofluids above the PV cell to transform solar radiation into energy. Their research used silver and gold nanoparticles to increase the PVT system's efficiency. Hossain et al. [22] did a comprehensive analysis of numerous elements of utilizing nanofluids for hybrid PVT systems, such as temperature drop, heat transfer coefficient, power generation, energy efficiency, overall efficiency, exergy efficiency, daily yield, entropy production, and exergy loss. Additionally, experimental, numerical, and combination investigations were included in the review, along with all new findings. After a thorough review, they concluded that multi-walled carbon nanotube (MWCNT)-based nanofluid is a better cooling fluid than oxide-based nanofluids. A nanofluid made from single-walled carbon nanotubes (SWCNT) increased daily yields and kept production costs low.

Adapting heat transfer fluids as cooling agents, particularly hybrid and ternary nanofluids, has received much attention [23]. Literature shows that PVT technology's efficiency increased by roughly 4% when ternary/hybrid nanofluid was used [24]. Adun et al. [25] assessed various effects of a PVT system employing a novel water-based Al_2O_3 -ZnO- FeO_4 ternary nanofluid. The maximum and total exergy efficiencies of PVT were determined to be 1.53% and 14.77%, respectively. The PVT system based on ternary nanofluid saved 19,948.04 kg CO_2 annually compared to 18,719.88 kg CO_2 when employing water as the heat transfer media. Kazemian et al. [26] studied the PVT system performance using four different types of hybrid nanofluids. The authors found that MWCNT-silicon carbide hybrid nanofluid shows the best cooling fluid among the considered hybrid nanofluids.

Based on the brief literature, it can be concluded that significant research has been conducted on PV and PVT systems, taking into consideration various factors, such as geometrical coordination, cooling fluid fluctuations, economic analysis, use, material properties, fluid properties, etc. However, due to Bangladesh's current energy crisis and price hikes, additional research is required to supply the country's excess energy demand through alternate energy sources. In addition, as far as the author is aware, no significant research on this topic has been undertaken with regression analysis and using Bangladeshi meteorological data. Additionally, a PVT system's efficiency is affected by various monthly weather-dependent factors such as irradiance, atmospheric temperature, wind velocity, etc. [27]. Besides this, the most recent nanofluid-based PVT research did not apply the appropriate nanofluid model, which is a vital issue with the efficacy of nanofluids [28]. Therefore, this study aims to enhance PVT performance in Dhaka, Bangladesh, employing MWCNT nanofluid with an appropriate nanofluid model and validated meteorological data based on Renewables.ninja that uses two primary data sources: (i) NASA MERRA reanalysis [29] and (ii) CM-SAF's SARAH dataset (Copyright 2015 EUMETSAT) [30,31]. Also, regression analysis is done for electrical and thermal efficiency, considering the Reynolds number and solar irradiation as input variables motivated by Rahman et al. [32]. In addition, the moth-wise PV cell efficiency, thermal efficiency, and total efficiency are

computed for varying Reynolds numbers and solar irradiation from 200 to 1000 W/m².

2. Mathematical modeling

2.1. Model description

The PVT system is depicted in cross-sectional form in Fig. 1. This system employs two different sorts of domains: solid and fluid. Glass, ethylene vinyl acetate (EVA), polycrystalline silicon cell, EVA, poly Vinyl fluoride (Tedlar), and thermal paste/adhesive comprise the solid domain. Two aluminum channel walls and one fluid domain compose a fluid domain. As a cooling fluid, MWCNT/water-based nanofluid is utilized. Consequently, the PVT system comprises a total of nine layers. Table 1 [9], Table 2 [33] and Table 3 [27] detail the dimensions, materials with design parameters, and thermophysical properties, respectively. 3D numerical simulation is conducted using finite element-based COMSOL Multiphysics software. Meteorological data for Dhaka, Bangladesh, is taken according to the Renewables.ninja [29–31]. Due to very thin layers and their negligible effects on thermal outputs, constant thermal characteristics are considered [34].

2.2. Governing equations and boundary conditions

Solid domains of PVT systems utilize the conduction heat transfer method. Conduction transmits thermal energy inside the solid domain for particle vibrations. The conduction equation for heat transmission between a photovoltaic (PV) cell and an aluminum wall of a fluid domain is

$$k_d \nabla^2 (T_d) = 0 \tag{1}$$

In the fluid domain, both conduction and convection heat transmission are utilized. Following are the ruling equations for the flow domain:

$$\nabla \cdot (\rho_{nf} \vec{V}_{nf}) = 0 \tag{2}$$

$$\nabla \cdot (\rho_{nf} \vec{V}_{nf} \vec{V}_{nf}) = -\nabla p + \mu_{nf} (\nabla^2 \vec{V}_{nf}) + \rho_{nf} g + S \tag{3}$$

$$\nabla \cdot (\rho_{nf} C_{p,nf} \vec{T}_{nf} \vec{V}_{nf}) = \nabla \cdot (k_{nf} \nabla \vec{T}_{nf}) \tag{4}$$

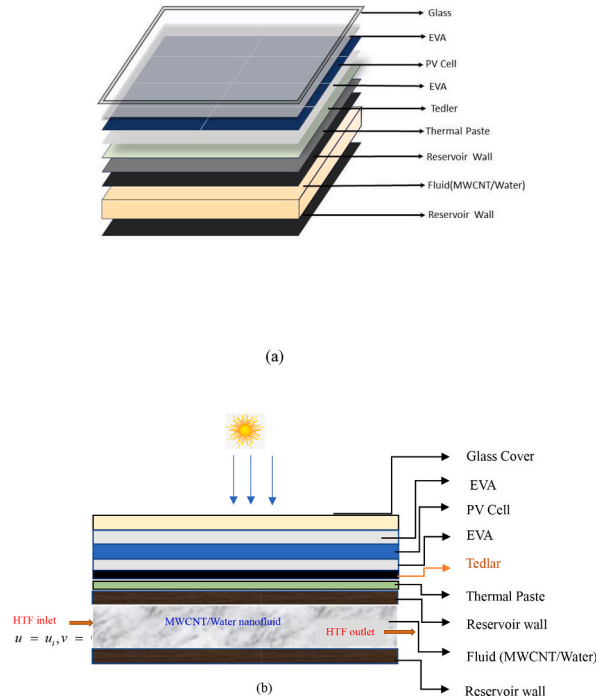


Fig. 1. Flat plate PVT collector: (a) exploded view. (b) Cross-sectional view.

Table 1
PVT layers material and thermophysical properties [9].

PVT elements	PVT layer	Dimensions (mm)	Density [kg/m ³]	Thermal Conductivity [W/(m.K)]	Heat capacity at constant pressure [J/(kg.K)]
Glass	Top part	1350 × 920 × 3	2450	2.00	500
EVA	Encapsulant	1350 × 920 × 0.8	950	0.311	2090
Silicon	Solar cell	1350 × 920 × 0.1	2329	148	700
Tedlar	Bottom part	1350 × 920 × 0.05	1200	0.15	1250
Thermal paste	Conductor	1350 × 920 × 0.3	2600	1.90	700
Aluminum	Collector wall	1350 × 920 × 1	2700	237	900
Fluid	MWCNT/Water nanofluid	1350 × 920 × 30	–	–	–

Table 2
Thermophysical properties of water and nanoparticles [33].

Property	Water	CNT
c_p	4179	650
ρ	997.1	1350
k	0.613	3500
β	2.1×10^{-4}	4.2×10^{-5}

Table 3
Designed parameters and their values [27].

Absorptivity of solar cell	0.9
Transmissivity of glass	0.95
Reynolds number	200–1000
PV cell efficiency at standard test conditions	0.14
Packing factor of solar cell	0.95
Coefficient of heat transfer from duct to water	500 W/m ² K
Coefficient of heat transfer from glass cover to ambient	(5.67 + 3.86 V) W/m ² K
Coefficient of heat transfer from glass cover to solar cell	9.24 W/m ² K
Coefficient of heat transfer from solar cell to tedlar	66 W/m ² K
Coefficient of heat transfer from tedlar to duct	8.1028 W/m ² K
Coefficient of heat transfer from duct to ambient	0.62 W/m ² K

Corresponding boundary conditions were used for the considered model are given below:
Inward heat flux occurs at the top glass surface

$$-k_g \frac{\partial T_g}{\partial z} = h_{ray,g \rightarrow env} (T_{amb} - T_g) \tag{5}$$

Radiative heat loss occurs on the PV's top surface according to Kazemian et al. [35].

$$-n \cdot q = \epsilon \sigma (T_{sky}^4 - T_g^4) \tag{6}$$

here, Stefan-Boltzmann constant, $\sigma = 5.670367 \times 10^{-8} \text{wm}^{-2}\text{K}^{-4}$.

Convective heat loss occurs at the heat exchanger's outer and lower borders based on Kazemian et al. [35].

$$-n \cdot q = h_{wind} (T_{wind} - T_g) \tag{7}$$

within the PVT module's outside perimeters:

$$\frac{\partial T_s}{\partial n} = 0 \tag{8}$$

At the upper and lower walls of the fluid domain:

$$u = v = w = 0 \tag{9}$$

At the duct interface of the solid and fluid domain

$$\left(\frac{\partial T_d}{\partial n}\right)_w = \frac{k_d}{k_w} \left(\frac{\partial T_d}{\partial n}\right)_d \quad (10)$$

$$\text{At the duct inlet: } u = u_i, v = 0, w = 0, \text{ and } T = T_i \quad (11)$$

$$\text{At the duct outlet: } p = 0 \quad (12)$$

2.3. Numerical process

The energy balance equation for glass to Tedlar and environment is [27].

$$E_c = Q_c + E_{th} + E_{el} \quad (13)$$

Overall, solar energy is obtained by the PVT unit in the following manner [27].

$$E_c = p_c \tau_g \alpha_c G A_c \quad (14)$$

Lost solar energy from the PVT module is calculated [27].

$$Q_c = h_c (T_c - T_{amb}) A_c \quad (15)$$

Here, McAdams (1954) provides the heat transfer coefficient h_c , which is applicable for wind speed, V between 0 and 10 m/s [9].

$$h_{wind} = 5.67 + 3.86V \quad (16)$$

The following equation is used to calculate the electrical energy produced from the conversion of the absorbed energy

$$E_{el} = \eta_{el} E_c \quad (17)$$

Where is the electrical efficiency is calculated based on Nahar et al. [9] as follows:

$$\eta_{el} = \eta_{ref} [1 - \beta_{ref} (T_c - T_{ref})] \quad (18)$$

Here η_{ref} represents the reference efficiency at standard conditions ($G = 1000 \text{ W/m}^2$, $T_{ref} = 25 \text{ }^\circ\text{C}$) and which is 0.13 based on Nahar et al. [36], β_{ref} denotes PV cell thermal coefficient that depends on PV cell materials, and is given as 0.0045/K for a silicon [37].

The absorbed thermal energy using the working fluid is analyzed by

$$E_{th} = \dot{m} C_{pw} (T_{out} - T_i) \quad (19)$$

\dot{m} denotes the mass flow rate, and the following equation is used to calculate it

$$\dot{m} = \rho U_0 A_{fc} \quad (20)$$

The preceding equations are utilized to calculate thermal efficiency and overall efficiency, respectively

$$\eta_{th} = \frac{E_{th}}{E_c}, \eta_{tot} = \frac{E_{th} + E_{el}}{E_c} \quad (21)$$

Reynolds number Re is defined below:

$$Re = \frac{\rho u_i d_h}{\mu} \quad (22)$$

where d_h is the hydraulic diameter of the fluid inlet.

2.4. Pre-assumptions

Pre-assumptions are taken for the 3D simulations of the considered PVT system associated with the boundary conditions as follows:

- Within the rectangular channel, fluid flow is laminar, incompressible, steady, uniform, and developed.
- A single-phase nanofluid model with thermal equilibrium features is considered to reduce computing complexity and time.
- The negligible thermal resistance of solid-to-solid contact is considered.
- The starting temperatures of all solid and fluid domains are identical to the surrounding temperature.
- Just the top surface of the glass lid will transfer heat into its surroundings through convection and radiation. The system's bottom surface and side walls are adiabatic.
- The upper EVA layer and glass cover are expected to be completely transparent such that the sun intensity on the top surface can be passed as a heat flux to the PV cell's top surface.

- Consideration is given to conduction heat transmission from the glass cover to the reserve wall and convection heat transfer from the reserve wall towards the fluid domain.

2.5. Nanofluid modeling

This numerical study, uses water-based MWCNT nanofluid based on Farbod et al. [38]. In their study, a 4% multiwalled carbon nanotube (MWCNT) with diameters less than 10 nm and a length of 5–15 μm was suspended in pure water using a two-step method. The stability of the water-based MWCNT nanofluid was tested using zeta voltage analysis (Zeta potential analysis). They revealed that the nanofluid is excellent stable as after 80 days at 50 °C, no sedimentation was found. The majority of past studies highlighted the importance of fluid composition and solid volume percentage. Most nanofluid heat transfer improvement experiments use base fluid with spherical nanoparticles. Particle size, shape, concentration, base fluid type, bulk fluid temperature, and others affect nanofluid heat transfer [28]. Before studying the convective heat transfer of nanofluids, its thermo-physical properties must be precisely determined. To make a nanofluid with a specific concentration (ϕ_{np}), a fixed quantity of nanomaterial (m_{np}) and base fluid (m_w) is required. equation (23) shows the relation to formulating 4% MWCNT/water nanofluid [39]. In this simulation of a single-phase homogeneous nanofluid, density and specific heat are estimated using the Pak and Cho model (equation (24)), and Xuan and Roetzel (equation (25)), respectively [40]. While the Esfe et al. [41] models, which were created for MWCNT/water nanofluid for the temperature variation of 25 °C–55 °C, are used to calculate thermal conductivity (equation (26)) and viscosity(equation (27)).

$$\phi_{np} = \frac{m_{np}}{m_{np} + m_w} \tag{23}$$

$$\rho_{nf} = \rho_{np}\phi_{np} + (1 - \phi_{np})\rho_w \tag{24}$$

$$C_{p,nf} = \frac{\phi_{np}\rho_{np}C_{p,np} + (1 - \phi_{np})\rho_w}{\rho_{nf}} \tag{25}$$

$$k_{nf} = \frac{(360.69 + T)k_w}{(405.59 - 11080\phi_{np})} \tag{26}$$

$$\mu_{nf} = (38.158\phi_{np} - 0.0017357T + 1.1296)\mu_w \tag{27}$$

2.6. Grid test

A grid refinement test was conducted at an irradiance of 1000 W/m², an inlet fluid velocity of 0.0005 m/s, and a temperature of 29 °C for optimal results. Discretizing the considered domain is essential meshing with the finite element method. The PV cell temperature (T_{cell} (°C)) and outlet temperature (T_{outlet} (°C)) of the fluid domain were used as control parameters, and the results of different mesh settings are shown in Fig. 2. Based on Fig. 2, the cell temperature and fluid flow outlet are virtually identical for normal and acceptable mesh settings, except for the time required. Therefore, the standard mesh configuration of mesh elements 858052 is utilized in this study.

2.7. Validation

Various numerical and experimental analysis studies are used to validate the precision of the numerical results. First, it is validated

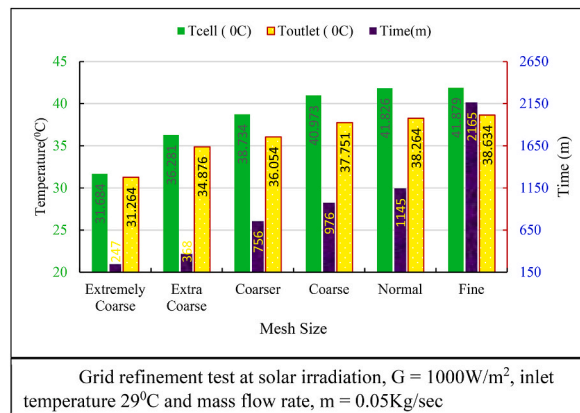


Fig. 2. Grid refinement test at solar irradiation, $G = 1000 \text{ W/m}^2$, inlet temperature 29°C and mass flow rate, $m = 0.05 \text{ kg/s}$.

with Fontenault and Gutierrez-Miravete [42] study. Using FEM-based COMSOL Multiphysics software, they analyzed the PVT performance of three different thicknesses of flow channel wall for an aluminum reservoir with variable flow velocity. More specifically, Water is used as a coolant fluid, and the authors validated this work for the thickness of the flow channel of 0.015 m, inlet flow velocity of 0.0002 m/s inlet, and ambient temperature of 298 K, wind velocity 1 m/s and irradiance of 1000 W/m^2 . The surface temperature plot is presented in Fig. 3(a) and compared with Fig. 4 of [42]. Second, it is validated with Nahar et al. [9], experimentation where electrical efficiency is used to measure of sensitivity. A three-dimensional PVT model with nine layers and a rectangular fluid field is used to evaluate these hypotheses by considering the following conditions: inlet velocity $u_0 = 0.0007 \text{ m/s}$, varying irradiance $R = 200\text{--}1000 \text{ W/m}^2$, inlet and ambient temperature $T = 34 \text{ }^\circ\text{C}$. The validation result is shown in Fig. 3(b). Third, with the experimental result of Al-Shamani et al. [16], it is validated for varying flow velocity at $G = 400 \text{ W/m}^2$, considering electrical efficiency as a controlling parameter. Table 4 displays the outcomes of this evaluation. It is evident from the above three comparisons that the results of this investigation and the published results coincide.

3. Result discussion

In this research, numerical simulation is employed to evaluate the monthly impact of the Reynolds number, considering solar irradiance, air temperature, and wind velocity on the 3D surface temperature, isotherm, outlet temperature, and cell temperature and efficiencies of a photovoltaic cell. The range of Reynolds numbers is considered from 200 to 1000 for every month and varying solar irradiation ($200 \text{ W/m}^2 \leq G \leq 1000 \text{ W/m}^2$). In COMSOL Multiphysics®, the governing equations are solved. The results of several cases are described in the sections that follow.

3.1. Month-wise variation of temperature, wind speed, and solar irradiation at Dhaka

Fig. 4 depicts the monthly variations in temperature, wind speed, and sun irradiance for the city of Dhaka. The performance of the PVT system depends highly on weather conditions. This research collected data from Renewables.ninja [29–31].for Dhaka, Bangladesh. Dhaka is located at 23.8103°N and 90.4125°E in terms of latitude and longitude, which impacts on temperature and solar radiation. Depending on latitude, the angle of solar radiation varies. From meteorological data, it can be determined that solar irradiation is at its peak (440 W/m^2) in April and lowest (260 W/m^2) in December, respectively, which is consistent with the ambient temperatures of those months, which are $29 \text{ }^\circ\text{C}$ and $18 \text{ }^\circ\text{C}$. Speculation can be made that the average temperature of a specific month varies with the solar irradiation. Although wind speed can be considered independent of temperature and irradiation, the highest wind speed of approximately 7 m/s is observed in May and July, and the lowest of 2 m/s is observed in November. As shown, the amount of solar irradiation is constrained in the winter since the Sun's rays fall at a low angle, which results in reduced power output. Since global solar radiation and air temperature are highly connected, increment radiation leads to a rise in atmospheric temperature.

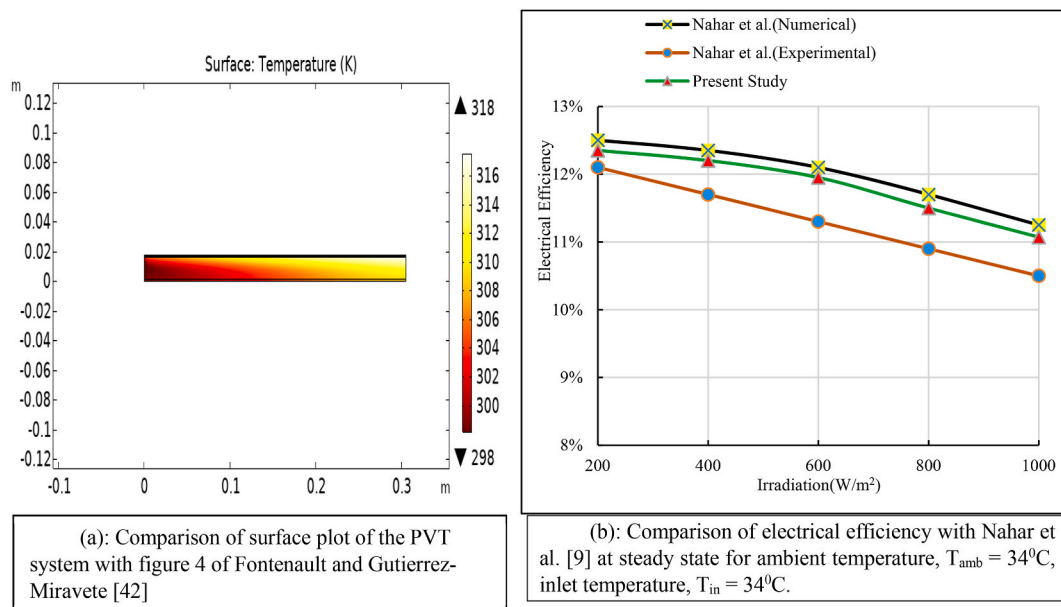


Fig. 3. (a) Comparison of surface plot of the PVT system with Fig. 4 of Fontenault and Gutierrez-Miravete [41] (b): Comparison of electrical efficiency with Nahar et al. [9] at steady state for ambient temperature, $T_{\text{amb}} = 34 \text{ }^\circ\text{C}$, inlet temperature, $T_{\text{in}} = 34 \text{ }^\circ\text{C}$.

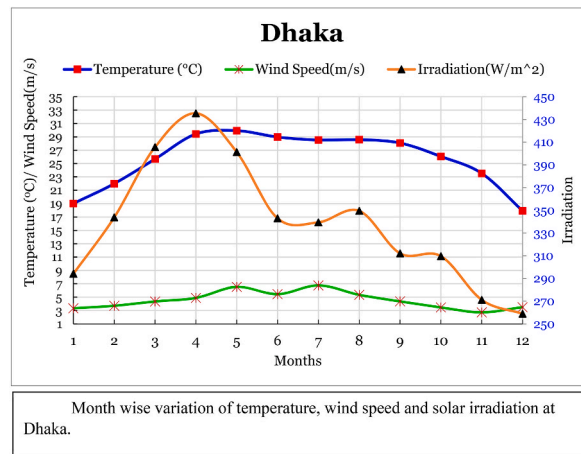


Fig. 4. Month wise variation of temperature, wind speed and solar irradiation at Dhaka.

Table 4

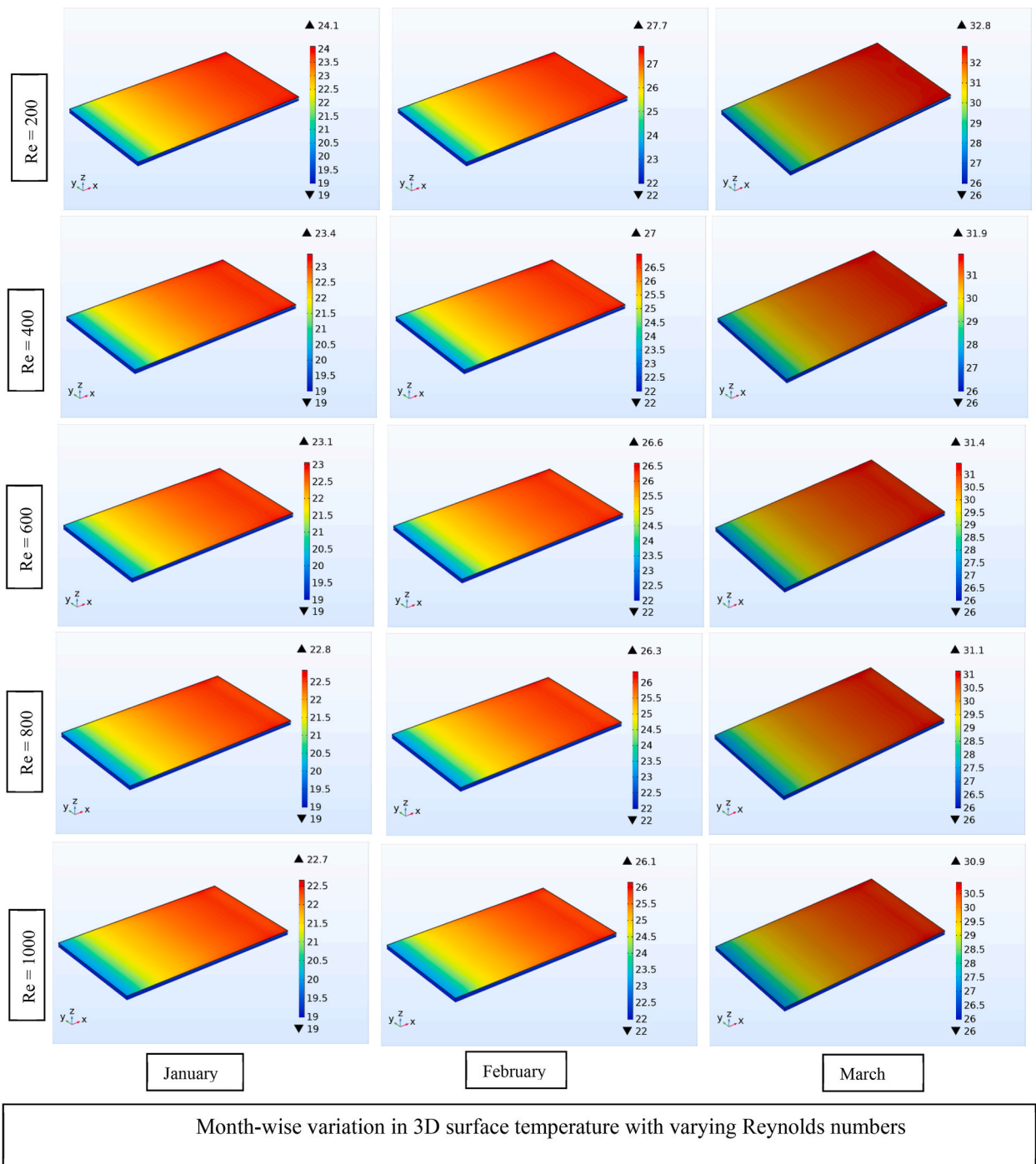
Electrical efficiency compared to Al-Shamani et al.'s experimental result [16] for varying inlet flow velocity at solar irradiation $G = 400 \text{ W/m}^2$.

Mass flow rate \dot{m} (kg/s)	Electrical Efficiency		Error%
	Al-Shamani et al. [16]	Present Study	
0.068	12.023	12.107	0.6986
0.102	12.273	12.358	0.6925
0.138	12.31	12.387	0.6255
0.170	12.467	12.541	0.5935

3.2. Effect of Reynolds number on 3D surface temperature

The simulation model examines how Reynolds number affects PV cell 3D surface temperature using numerical analysis. A layer-by-layer parametric study and numerical simulation were done for the PVT system. A 3D surface analysis of the entire PVT system, which consists of nine layers, has been performed. The monthly effect in Dhaka city is shown in Fig. 5 for the Reynolds number fluctuation from 200 to 1000. Wind speed and solar irradiation change every month, which affects the ambient temperature of that month.

It is seen from Fig. 5 that the wind speed for January is 3 m/s, the temperature is 19 °C, and the normal solar radiation is 294 W/m². At a Reynolds number of 200, the temperature ranges from a low of 19 °C, the ambient temperature, to a high of 24.1 °C. Raising the Reynolds number to 400 caused the PV surface temperature to drop from its previously high state to 23.42 °C. This is because the fluid velocity increased at higher Reynolds numbers, and temperature transportation was faster in the fluid flow. Inertial and viscous forces regulate fluid flow; the relative significance of these two activities has a major effect on a fluid's ability to transfer heat and flow. Due to heat transfer, the PVT cell's higher temperature was decreased. In the PVT system, convection heat transfer occurs everywhere except in the fluid layer, which experiences conduction heat transfer. Convective heat transfer rises with the increasing flow velocity. The surface temperature decreases as the Reynolds number rises due to the increased heat extraction rate caused by the flow's increasing inertial activity. The higher solar irradiation and temperature in February accounted for a little increase in temperature from January. The same factor continues to cause the surface temperature to rise in the consecutive months of March. The maximum amount of solar radiation occurred in April, whereas the highest temperatures and wind speeds occurred in May. Increased solar irradiance, a rise in ambient temperature and wind velocity, increase the heat transfer within the PV surface. The more significant flow velocity caused the higher surface temperature to decrease as the Reynolds number increased. In June, the PV cell's maximum surface temperature was reduced to 34.8 °C at the lowest $Re = 200$ and 33.3 °C at the highest $Re = 1000$ due to a significant fall in wind speed and solar irradiance. In July, solar energy and temperature decreased slightly, resulting in a modest drop in temperature to 33.5 °C at $Re = 200$. In August, the surface temperature rose to 34 °C due to a little increase in ambient temperature and solar irradiance. From August through December, the environmental temperature, wind velocity, irradiance, and PV cell surface temperature decrease steadily. The higher surface temperature of PV is 22.7 °C at $Re = 200$ at the solar irradiance's lowest point (260 W/m²) in December. In April, when solar energy reaches its maximum level (440 W/m²), the PV surface temperature increases to 35.7 °C. April and December have the highest and minimum temperatures, respectively. At lower Re values, the decrease in cell temperature is more evident, while it becomes less pronounced at high Re values. The cause of this spectacle is evident in Fig. 5, which shows that the rate of heat transfer proportionally increases with Reynolds number.

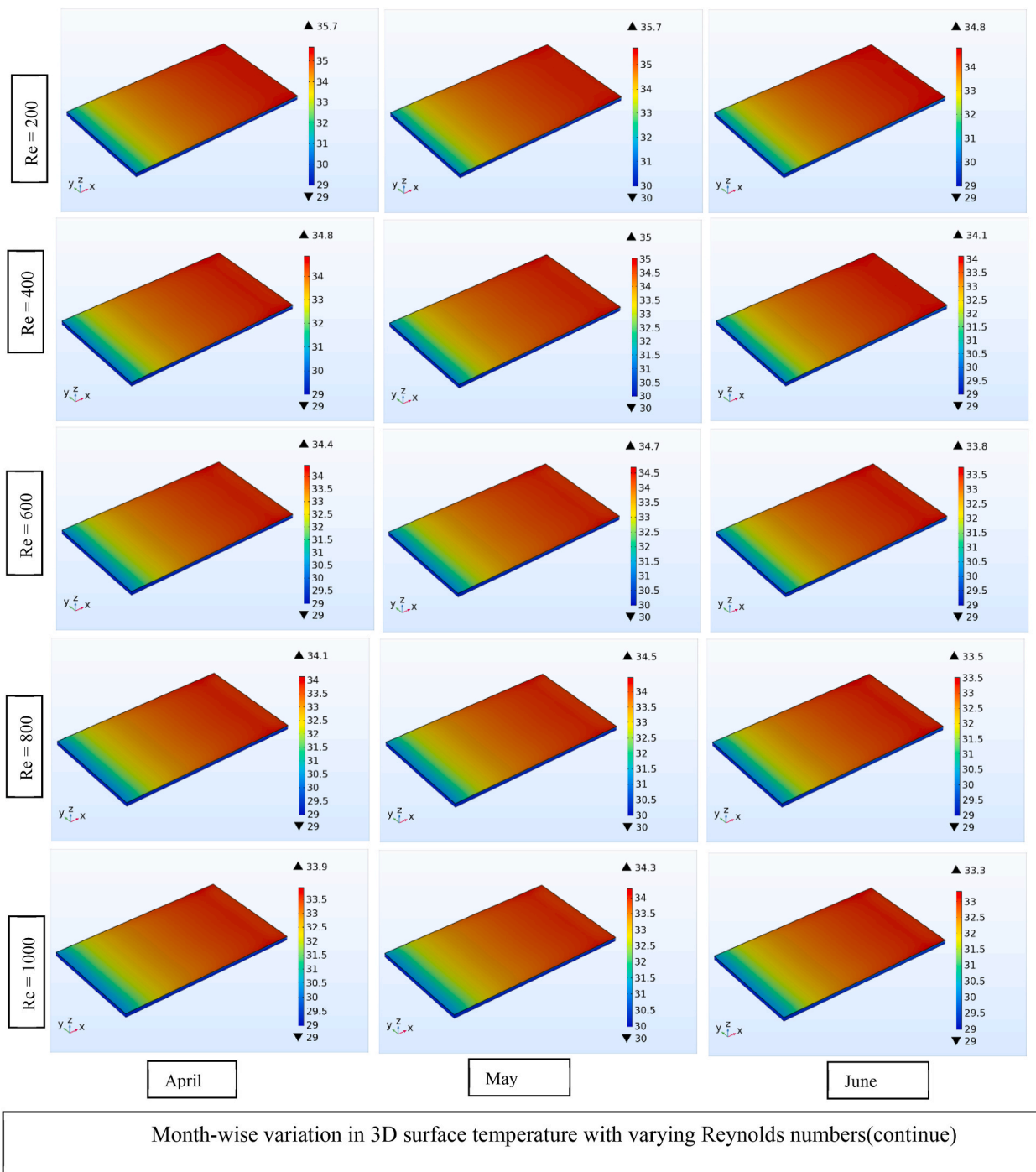


Month-wise variation in 3D surface temperature with varying Reynolds numbers

Fig. 5. Month-wise variation in 3D surface temperature with varying Reynolds numbers.

3.3. Effect of Reynolds number on isotherms

In this study, isothermal lines are presented along with the surface temperature due to clearly visualizing the temperature distribution within the connecting points. As depicted in Fig. 6, the isothermal lines vary monthly. In January, the wind velocity, solar irradiation, and ambient temperature were comparatively less than in the months following. Isotherms are densely gathered in this month because, with a fixed Reynolds number, temperature dissipation is less at the observed lower temperature of 19.1 °C. The



Month-wise variation in 3D surface temperature with varying Reynolds numbers(continue)

Fig. 5. (continued).

isotherms are distributed more widely as the surface temperature of PVT cells continues to rise, leading to an increase in temperature dissipation. Now, the temperature drops because of increased fluid velocity for increasing the value of Re. With a Re increase from 200 to 1000, the maximum temperature of the PVT cell reduced from 24 °C to 22.6 °C. The isotherms are densely gathered over the PVT surface as Re increases, indicating less temperature dissipation. A comparable occurrence is seen for all other months. The variation in isotherm was more significant in February due to the higher temperature, which increased marginally from January. The surface temperature continues to rise till May because of higher weather factors, resulting in more scattered isotherms. The most significant amount of solar radiation occurred in April, whereas ambient temperature and wind velocity peaked in May. Due to the greatest

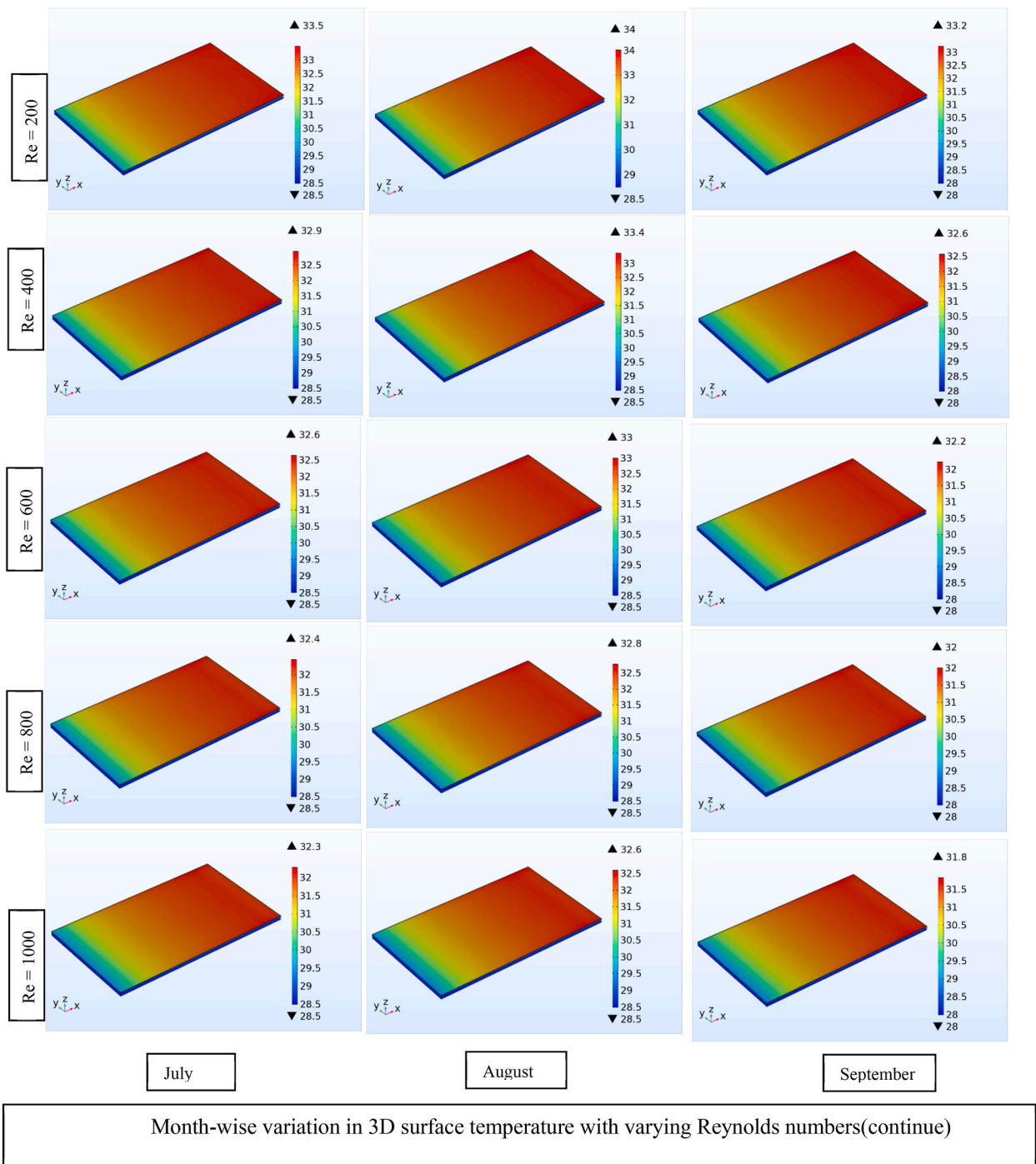


Fig. 5. (continued).

temperature recorded for all Re values in May, the isothermal contour line is also the most dispersed. From the 35.5 °C recorded in May, the temperature declined to 34.7 °C and 33.4 °C in June and July due to a significant fall in solar irradiation and the surrounding temperature. This decrease in cell temperature caused isotherms to condense. In August, the surface temperature increased to 33.9 °C, resulting in more variation in isotherm. The operating temperature in the PV system has a pivotal role that changes monthly, even with other well-regulated factors. Due to a decrease in irradiance and environment temperature from August to December, the PV panel’s surface temperature decreases, resulting in less variable isotherms and a slower rate of temperature dissipation. Some speculation can be made that as Reynolds number increases, natural convection decreases, so temperature dissipation is less prominent. Reynolds

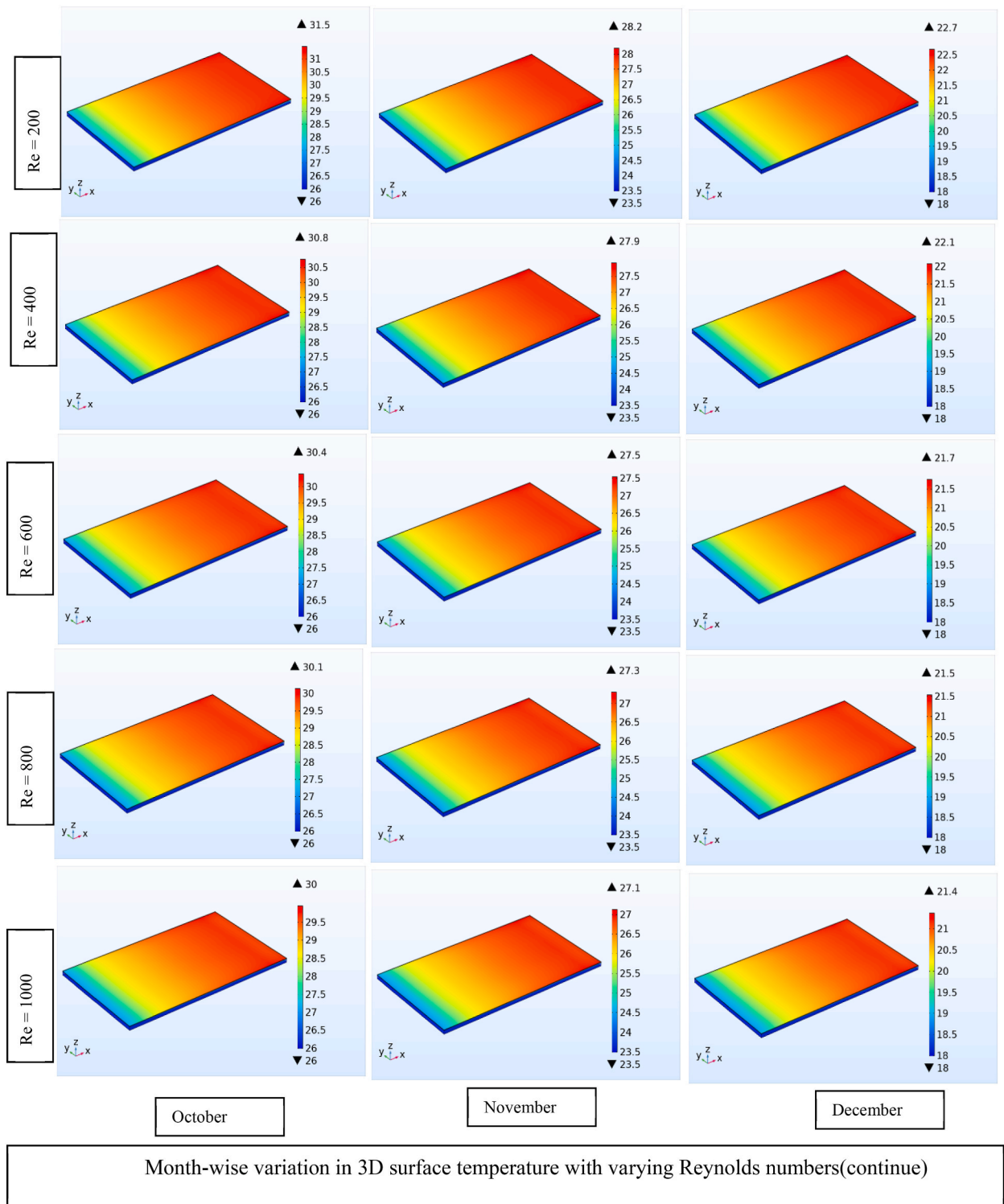


Fig. 5. (continued).

number strongly influences heat transmission and isothermal contour lines. Another notion holds that the cell temperature decreases as the Reynolds number rises because inertial flow activity accelerates heat loss. Fig. 6 shows that cell temperature decreases faster at lower Re than higher Re. Flow velocity greatly influences the isotherm of a fluid domain, which shows the convective heat transfer rate in the fluid. Isotherms are highly scattered at the maximum temperature recorded in May, whereas in December when solar irradiation

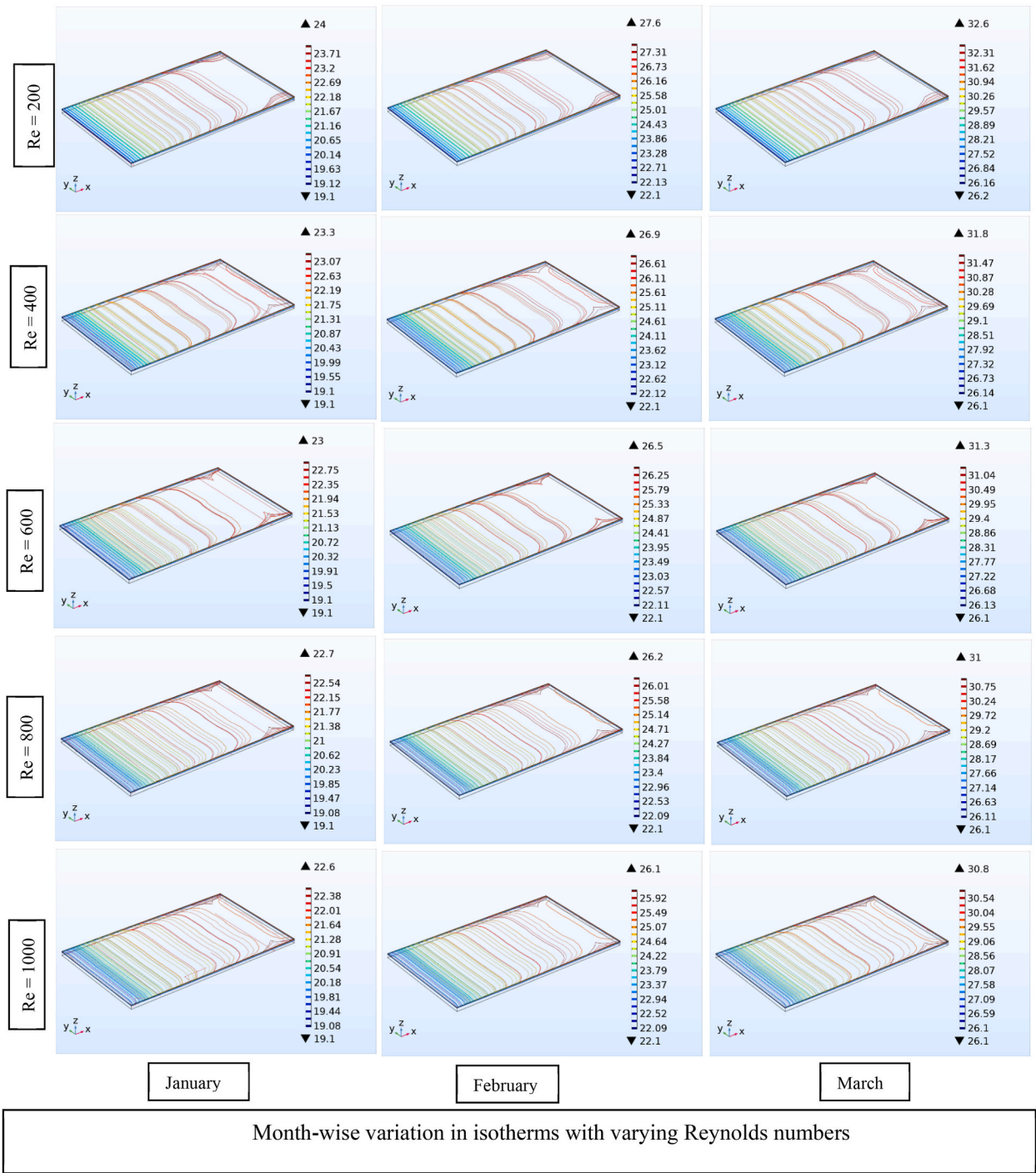


Fig. 6. Month-wise variation in isotherms with varying Reynolds numbers.

and ambient temperature were at their lowest points, they were more concentrated. According to the analysis, the low Reynolds number and the PV cell surface temperature play a significant role in the fluid’s ability to dissipate heat. So, by decreasing Re and increasing temperature, more scattered isotherms can be generated.

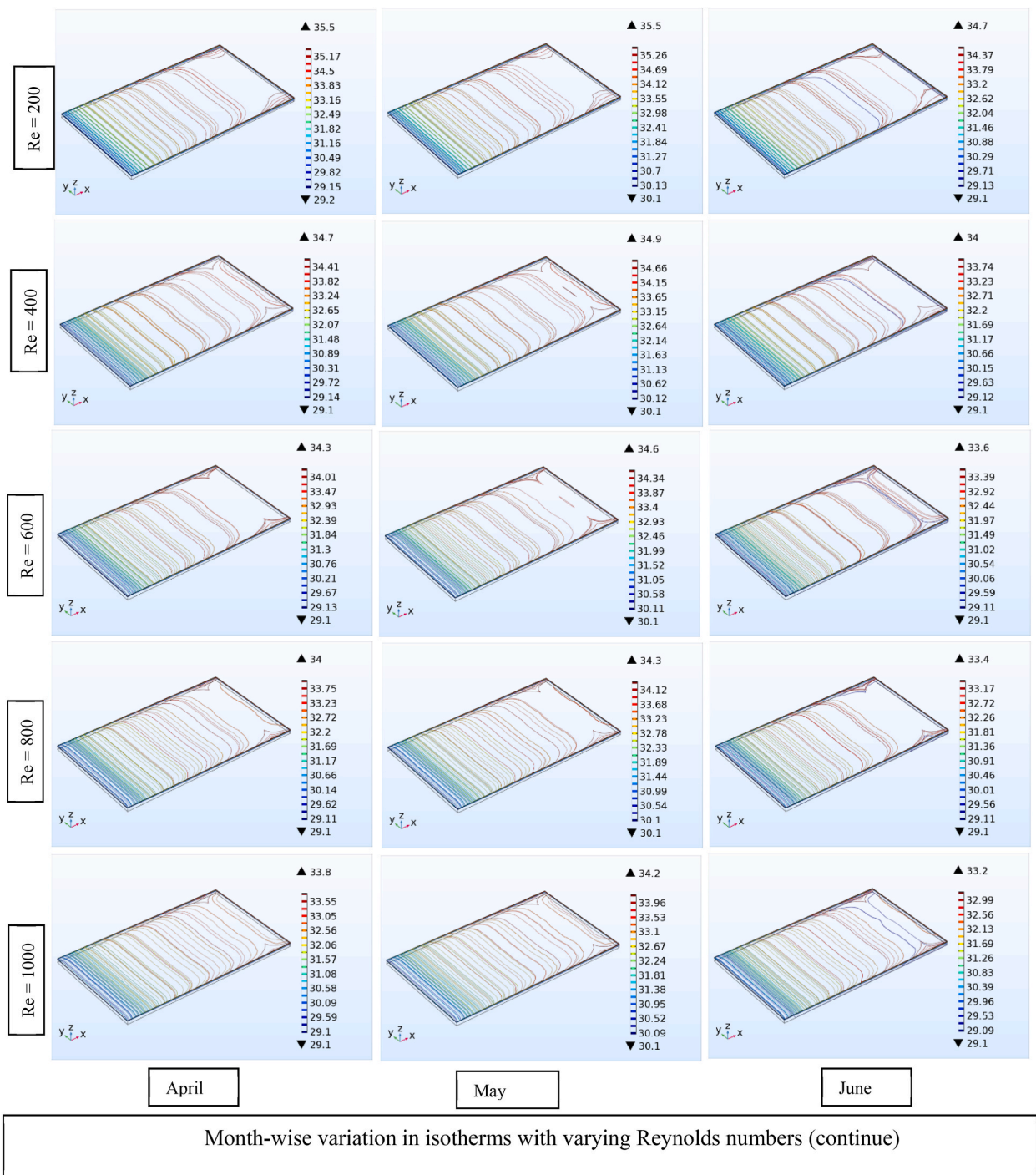


Fig. 6. (continued).

3.4. Month-wise effect of Reynolds number on outlet temperature

The outlet temperature of the fluid domain (°C) for the monthly influence of the Reynolds number is shown in Fig. 7. The increasing value of wind velocity, ambient temperature, and irradiation cause fluid outlet temperature variation. In May, the outlet temperature was maximum (31 °C) because of maximum wind velocity (7 m/s) and higher ambient temperature (30 °C). Due to the slightly lower ambient temperature than in May, June had the second-highest temperature, at 29 °C. Outlet temperature was observed to be lowest at 18.5 °C in December because of the minimum wind velocity, ambient temperature, and irradiation found. The higher outlet fluid

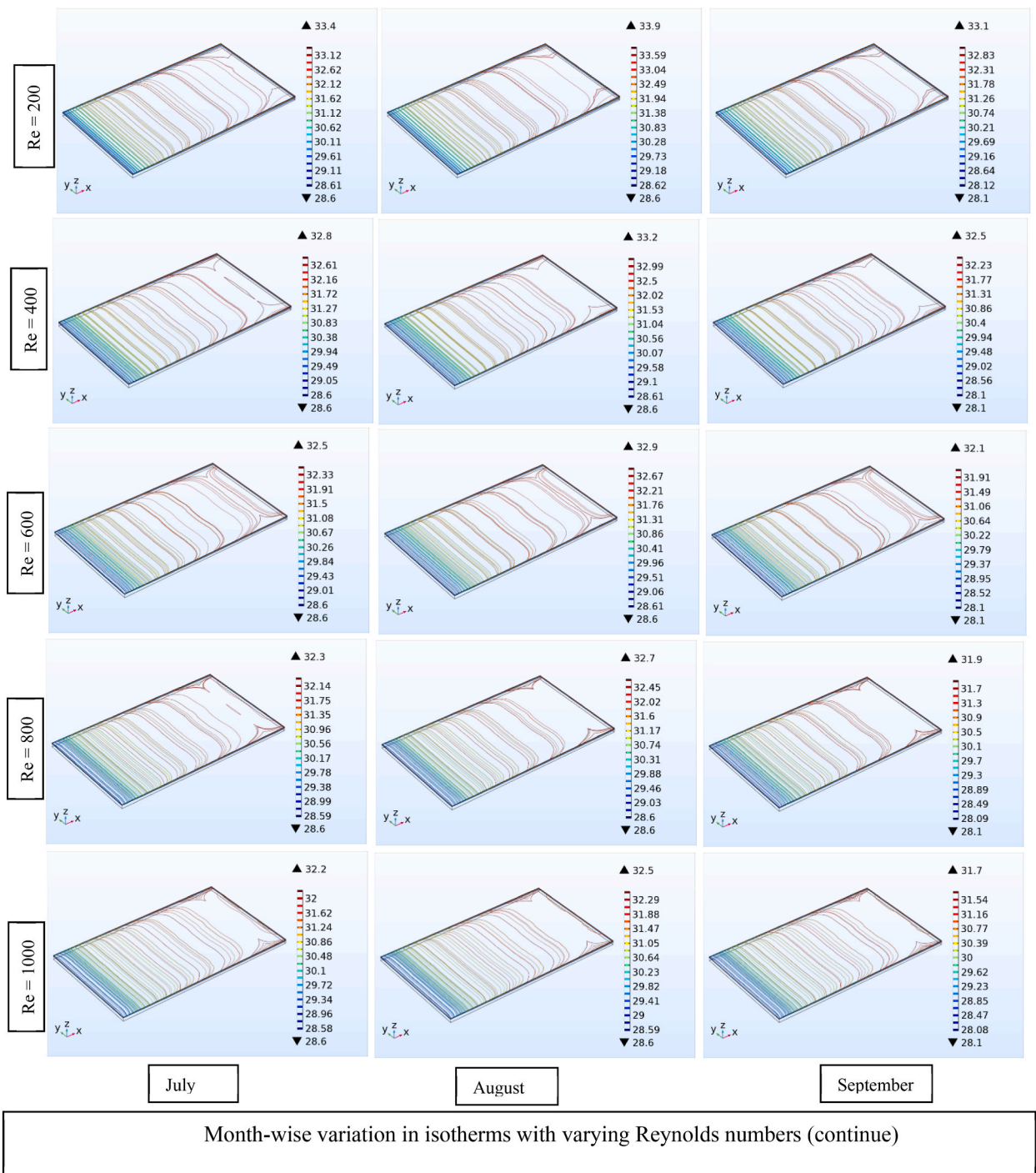


Fig. 6. (continued).

temperature depicts that the temperature dissipation is higher in fluid. The heat transfer rate increases with outlet temperature, helping to raise the PV cell's total efficiency.

3.5. Month-wise effect of Reynolds number on PV cell temperature

The output power and electrical efficiency of a PVT system are both significantly affected by the temperature of the solar cells. Fig. 8 depicts the monthly effect of the Reynolds number on PV cell temperature. The electrical performance is adversely impacted by

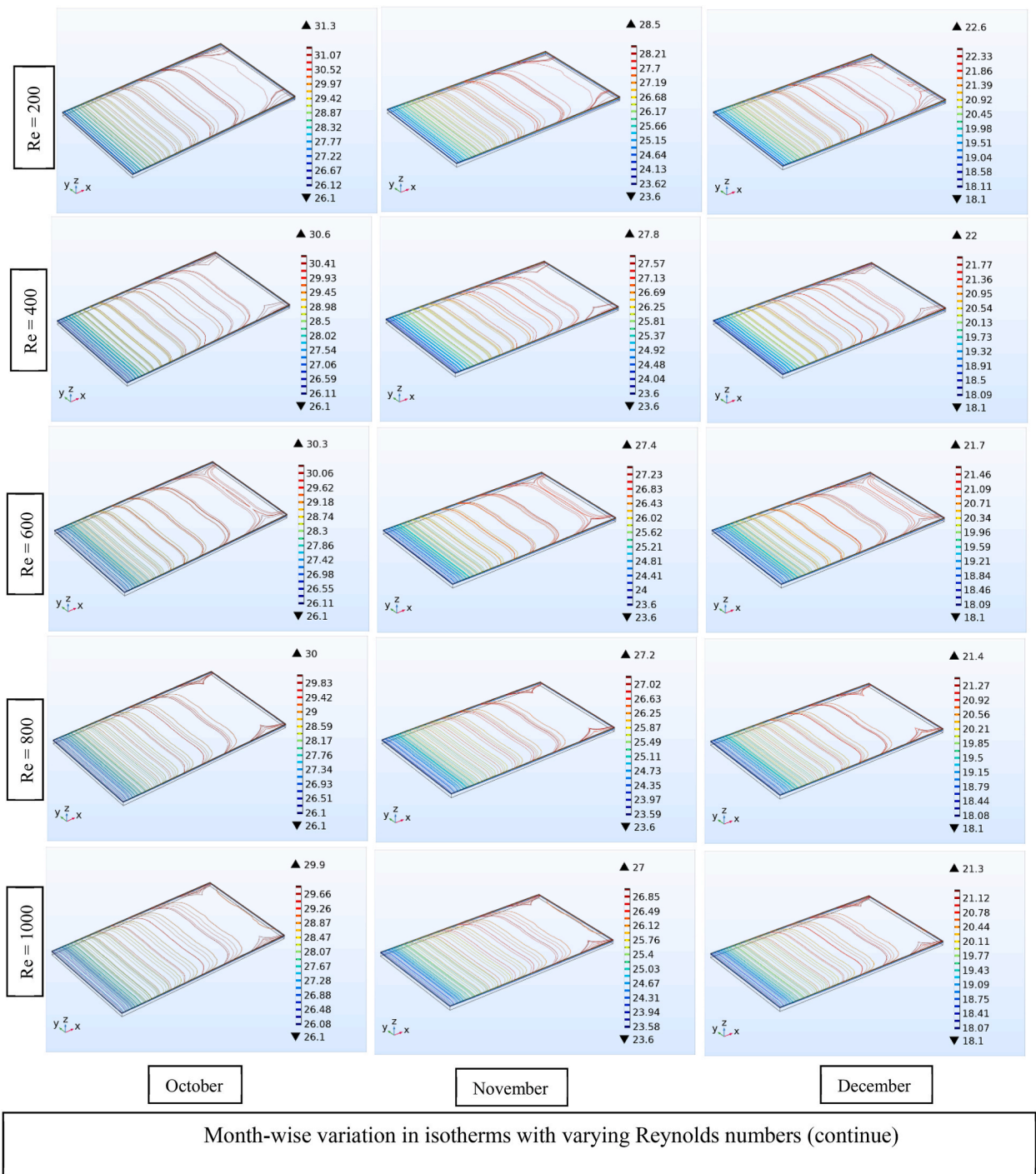


Fig. 6. (continued).

an escalation in the PV module temperature since the electrical efficiency declines significantly. The diagram illustrates how the encircling environment, wind velocity, and incident radiation influence the temperature of a PV cell. The temperature of solar cells increases with high irradiation which is the prime reason for the maximum cell temperature of 35 °C in May. After April and May, the highest temperature is 34.5 °C. The lowest cell temperature of 22 °C was observed in December due to minimum weather factors. Observation shows that by keeping the month constant, for gradually increasing values of Re, PV cell temperature slightly follows a decreasing trend. This is due to the fact that flow velocity has a significant impact on the temperature profile of a flow field, which in turn controls the rate of convective heat transfer. Because the PV cell gained the fluid’s conduction-acquired temperature as the

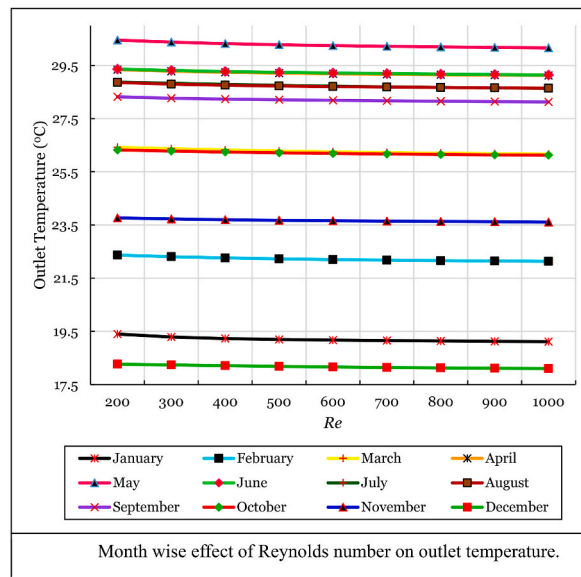


Fig. 7. Month wise effect of Reynolds number on outlet temperature.

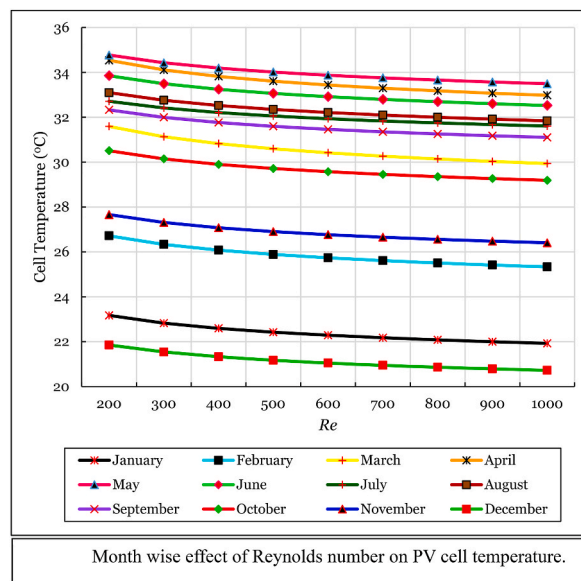


Fig. 8. Month wise effect of Reynolds number on PV cell temperature.

Reynolds number increased. Following temperature acquisition, convective heat transfer led to increased fluid movement. In all months, when the Reynolds number grew, heat transmission increased, leading to a reduction in PV cell temperature.

3.6. Month-wise effect of Reynolds number on electrical efficiency

Fig. 9 shows the month-wise the Reynolds number effect on electrical efficiency. Increasing Re from 200 to 1000 consequently improves the module’s electrical efficiency. When Re is high, the cell temperature is less, consequently, the electrical efficiency is high. December is the month with the lowest temperature, 22 °C, resulting in the highest electrical efficiency of 12.75%. Solar irradiation and ambient temperature were lowest in Dhaka this month. PV solar cells had a minimum electrical efficiency of 11.95% in May due to the maximum cell temperature of 35 °C, which occurred for high solar irradiation and ambient temperature. As a result, there is a negative correlation between PV cell temperature and power output.

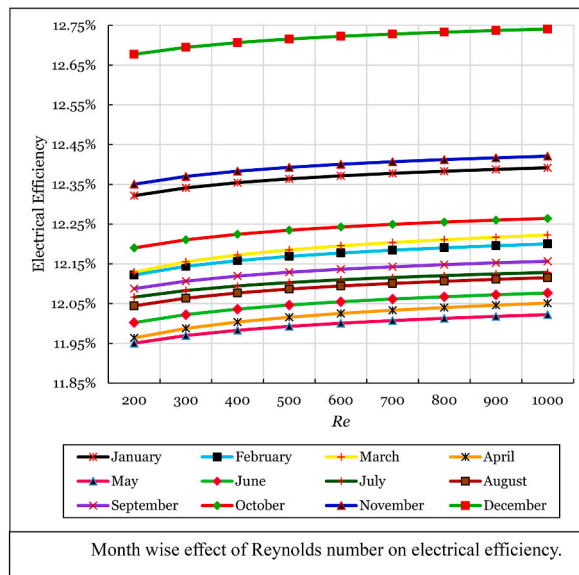


Fig. 9. Month wise effect of Reynolds number on electrical efficiency.

3.7. Month-wise effect of Reynolds number on thermal efficiency

The difference in thermal efficiency because of Reynolds number and month variation is depicted in Fig. 10. The temperature at the PVT cell's outlet has a considerable impact on the cell's overall thermal performance. In Dhaka city, the outlet temperature is at its maximum in May, resulting in higher thermal efficiency. Increased thermal efficiency is perceived in March and April, although May has the maximum thermal efficiency. The reason for this is realized in Fig. 4, which manifests the high radiation, wind velocity, and ambient temperature in these months. Again, in August and September, high thermal efficiency is noticed because of higher wind velocity. The coefficient of heat transfer increases with the wind speed, which means that more heat can be transferred when the wind speed is high. Thermal efficiency was lower in the colder months of November, December, and January due to less ambient temperature and other weather factors. Reynolds number regulates the system's heat transfer qualities directly, which has a substantial effect on PVT performance, especially thermal efficiency. In general, when Re is increased, both electrical and thermal efficiencies improve, although the improvement in thermal efficiency is much more noticeable. That related to the efficiency change from 40% to 75% for Re change from 200 to 1000 in July. A similar phenomenon is observed in all other months accordingly.

3.8. Month-wise effect of Reynolds number on total efficiency

Energy efficiency is the ratio of the input energy to the outgoing energy of a system. Fig. 11 depicts the monthly effect of Re on the overall efficacy of the PVT system. The total energy available to a system is determined by adding the electrical and thermal

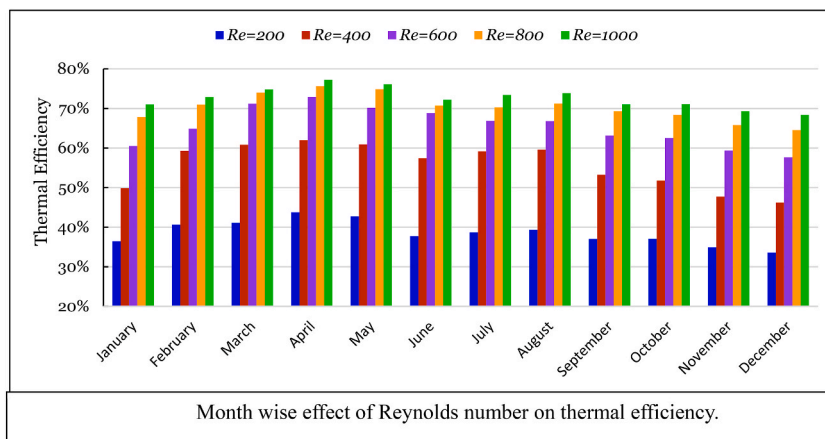


Fig. 10. Month wise effect of Reynolds number on thermal efficiency.

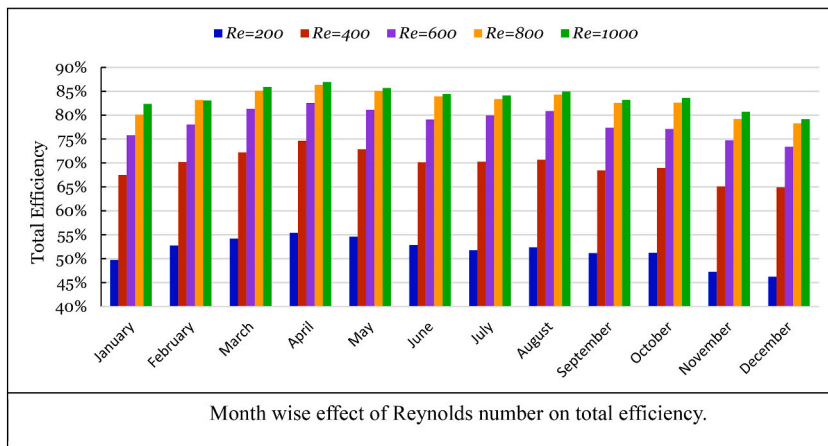


Fig. 11. Month wise effect of Reynolds number on total efficiency.

efficiencies. With increasing solar irradiance, the entire energy output of the PV cell increases. Increased irradiance can increase the voltage and current of the PV system. Total efficiency is highest in April as solar irradiation was highest, as perceived from Fig. 4. Reynold number significantly impacts PVT performance, and total efficiency rises as Re increases. Fig. 8 demonstrates that the flow with the highest Re of 1000 in April and May, along with the maximum temperature, irradiation, and wind velocity, results in the highest total efficiency of up to 86%. The total efficiency of the PV cell is found to be high in the consecutive months of March through May and August through September; conversely, thermal efficiency dropped from November through December, when the most negligible radiation is seen.

3.9. Combined effect of Re and G on electrical efficiency

Fig. 12 shows how the electrical efficiency of the PVT cell varies as a function of the Reynolds number (Re) and solar irradiation (G). According to equation (18), as the temperature of the PVT cell (T_c) rises, so does its electrical efficiency. April was chosen for the analysis because it was observed that the sun’s irradiance and the ambient temperature were at their zenith during this month. Reynolds number is a forced convection parameter proportional to the inlet velocity of the PVT cell. Increasing the Reynolds number raises the velocity of the entering fluid, which in turn raises the velocity of the leaving fluid and the rate of heat transfer. Cooling, reduced cell temperature, and enhanced electrical efficiency result from this enhancement in heat transport. At $Re = 1000$, the electrical efficacy is at its peak, while at $Re = 200$, it is at its minimum. This conforms to the empirical finding.

Solar irradiation is the sun’s heat flux; as solar irradiation increases, so does the heat flux in the PVT surface plate, increasing cell

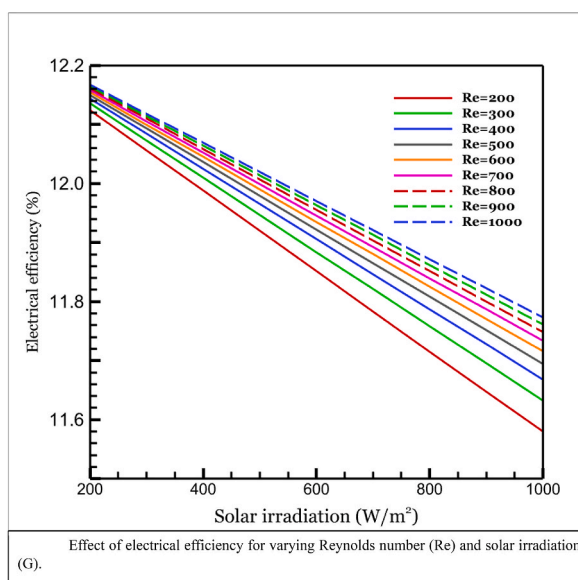


Fig. 12. Effect of electrical efficiency for varying Reynolds number (Re) and solar irradiation (G).

temperature. Hence, electrical efficiency falls as solar irradiance increases. The empirical conclusion indicates that when solar irradiance ($G = 200 \text{ W/m}^2$) is held constant, the electrical efficiency decreases by 0.35% as Re increases from 200 to 1000. At $G = 1000 \text{ W/m}^2$, which is the highest solar irradiance of our observation, it decreased by 1.6 %, as Re increased from 200 to 1000. A comparative trend can be demonstrated by varying the solar irradiance while maintaining the fluid velocity, Re, constant. For the maximum Re = 1000 value from experimental measurements, the electrical efficiency increases by 0.4% for every 100 W/m^2 increase in solar irradiance, while for the lowest Re = 200 value, the percentage is 0.56%. Overall, the results suggest that elevated cell temperature reduces the PVT system's electrical efficiency.

3.10. Combined effect of Re and G on thermal efficiency

Fig. 13 uses April's data to show how Re and G, the quantity of solar energy received, affect the PVT cell's thermal efficiency. Theoretically, thermal efficiency is defined as the percentage of available heat converted into practical work. According to equation (21), a positive relationship exists between an increase in thermal energy absorbed and a decrease in total energy and the thermal efficiency of a system. This suggests that a greater quantity of absorbed thermal energy can result in a more efficient system. However, reducing total energy consumption can also improve thermal efficiency. Increasing the mass flow rate of a system can increase the quantity of thermal energy absorbed, according to equation (19). A more significant Reynolds number indicated an increase in fluid velocity, which led to a rise in mass flow rate, increasing thermal efficiency (E_{th}). According to equation (14), solar irradiation is proportional to the total energy of a system. This indicates that a rise in solar irradiance increases the total energy input to the system. Thermal efficiency declined as the total quantity of energy increased. This relationship implies that as solar irradiance increases, the system's thermal efficiency may decrease.

Based on numerical analysis, it was shown that when solar irradiance was held constant throughout all data, the increase in Reynolds number from 200 to 1000 caused a 5.6% increase in thermal efficiency. Similarly, when a constant input velocity was maintained for all observations of the Reynolds number, the thermal efficiency rose by 9.9% as solar irradiance climbed from 200 to 1000 W/m^2 . These results are essential for comprehending the interaction between various variables in solar energy systems, particularly in improving the PVT system. Researchers and practitioners might potentially maximize the design and operation of solar energy technology by finding the correlations between solar irradiance, Reynolds number, and cell temperature.

3.11. Regression analysis of electrical and thermal efficiency

Electrical efficiency (η_{el}), illustrated in Fig. 12, and thermal efficiency (η_{th}), illustrated in Fig. 13, are mathematically correlated with the independent variables Reynolds number (Re) and Solar irradiation (G). The independent variables range from 200 to 1000. The proposed correlations are presented by equations (28) and (29) and as follows:

$$\eta_{el} = 1.54\text{Re}^{-6} - 5.5G^{-6} + 0.121942, R^2 = 0.986 \quad (28)$$

$$\eta_{th} = 5.04\text{Re}^{-5} - 8.5G^{-5} + 0.766293, R^2 = 0.849 \quad (29)$$

From the above regression equations and correlation coefficient, it is evident that electrical and thermal efficiency both positively depend on Reynolds number and negatively depend on solar irradiation. In equation (28), the R^2 value of 0.986 indicates that the regression model determines 98.6% of the variance in electrical efficiency. This high value of R^2 exhibits that the regression model is a good fit for the empirical data and that the Reynolds number and solar irradiation in the model are strongly related to the electrical efficiency. Similarly, in equation (29), the R^2 value of 0.849 indicates that the regression model determines 84.9% of the variance in the thermal efficiency. This relatively high value of R^2 exhibits that the regression model is a good fit for the empirical data and that the Reynolds number and solar irradiation in the model are strongly related to thermal efficiency. Therefore, the model with an R^2 of 0.986 is likely a much better fit for the data than the model with an R^2 of 0.849, as it explains a higher proportion of the variance in the Reynolds number and solar irradiation.

4. Conclusion

A parametric analysis of a PVT system performance is conducted utilizing nanofluid and a numerical model is analyzed in this study. The monthly effect of the Reynolds number and solar irradiation have been observed. Some inferences were taken from the analysis, with the monthly weather change resulting in the change of surface temperature, isotherms, outlet temperature, cell temperature, and consequently system efficiency. The key conclusions of the research are:

- During the months with the highest solar irradiance and wind velocity, the PVT system's cell temperature, outlet temperature, and thermal efficiency are at their peak.
- The performance of PV cells is higher in December. Both electrical and thermal efficiency positively depend on Reynolds number and negatively depend on solar irradiation.
- At any given Re, April is the best month for thermal and overall performance, followed by March and May.
- Electrical efficiency increased by 8% from May to December.

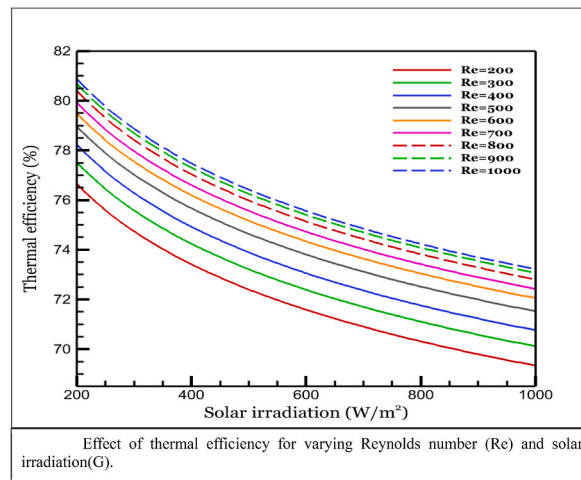


Fig. 13. Effect of thermal efficiency for varying Reynolds number (Re) and solar irradiation(G).

- With rising Reynolds number cell temperature decreased and overall PVT performance enhanced. But reverse situation is observed for rising solar irradiation.

This study can be used to install PVT systems and other relevant renewable solar energy sources in Dhaka, Bangladesh, considering the meteorological effect. At the end, those working in solar thermal heating, building-integrated photovoltaics, thermal science, and industrial and residential cooling system areas would benefit from this study.

CRedit authorship contribution statement

A.K. Azad: Writing – review & editing, Writing – original draft, Visualization, Validation, Software, Resources, Methodology, Formal analysis, Conceptualization. **Salma Parvin:** Supervision, Project administration, Methodology, Conceptualization. **Tahiya Hossain:** Writing – original draft, Visualization.

Declaration of competing interest

On behalf of all authors, I declared that we have no known competing financial interests or personal relationships that could have appeared to influence the work reported in this paper.

Nomenclature

A_c	Area of PV cell(m ²)
A_{fc}	Cross sectional area of inlet(m ²)
C_p	Specific heat (J/(Kg.K))
C_{pw}	Specific heat of water(J/(Kg.K))
E_c	Total PV cell energy (W)
E_{el}	Electric power (W)
E_{th}	FEM Thermal energy absorbed by the fluid (W) Finite element method
G	Solar irradiance(W/m ²)
HTF	Heat transfer fluid
h_c	IEA Heat transfer coefficient(W/(m ² K)) International energy agency
k_d	Thermal conductivity of the duct(W/(m/K))
k_g	Thermal conductivity of the glass (W/(m/K))
k_w	Thermal conductivity of the fluid(W/(m/K))
LNG	Liquefied natural gas
MWCNT	Multi-walled carbon nanotube
\dot{m}	Mass flow rate (kg/s)
n	Normal to the surface
PV	Photovoltaic
p_c	Packing factor
p	Pressure (Pa)

Q_c	Heat loss(W/m^2)
q	Heat flux(W/m^2)
Re	Reynolds number
SWCNT	Single-walled carbon nanotube
T_{amb}	Ambient temperature ($^{\circ}C$)
T_c	PV cell temperature ($^{\circ}C$)
T_d	Duct temperature ($^{\circ}C$)
T_g	Glass temperature($^{\circ}C$)
T_i	Inlet temperature of the fluid($^{\circ}C$)
T_{out}	Outlet temperature of the fluid ($^{\circ}C$)
T_{ref}	Reference temperature ($^{\circ}C$)
T_w	Fluid temperature ($^{\circ}C$)
u, v, w	Fluid velocity (m/s)
U_0	Inlet flow velocity (m/s)
V	Wind velocity (m/s)

Greek Symbols

β_{ref}	Thermal coefficient
μ	Fluid dynamic viscosity (Pa s)
ν	Fluid kinematic viscosity (m^2s^{-2})
ρ	Fluid density(kg/m^3)
η_{el}	Electrical efficiency
η_{th}	Thermal efficiency
η_{tol}	Overall efficiency
η_{ref}	Cell reference efficiency
τ_g	Glass emissivity

References

- [1] S. Vaishak, P.V. Bhale, Photovoltaic/thermal-solar assisted heat pump system: current status and future prospects, *Sol. Energy* 189 (2019) 268–284, <https://doi.org/10.1016/J.SOLENER.2019.07.051>. Sep.
- [2] M.M. Fouad, L.A. Shihata, E.S.I. Morgan, An integrated review of factors influencing the performance of photovoltaic panels, *Renew. Sustain. Energy Rev.* 80 (2017) 1499–1511, <https://doi.org/10.1016/j.rser.2017.05.141>. Dec.
- [3] A.W. Kandeal, et al., Photovoltaics performance improvement using different cooling methodologies: a state-of-art review, *J. Clean. Prod.* 273 (2020) 122772, <https://doi.org/10.1016/J.JCLEPRO.2020.122772>. Nov.
- [4] A.K. Azad, S. Parvin, Bibliometric analysis of photovoltaic thermal (PV/T) system: from citation mapping to research agenda, *Energy Rep.* 8 (2022) 2699–2711, <https://doi.org/10.1016/J.EGYR.2022.01.182>. Nov.
- [5] S.A. Kalogirou, S. Karellas, V. Badescu, K. Braimakis, Exergy analysis on solar thermal systems: a better understanding of their sustainability, *Renew. Energy* 85 (2016) 1328–1333, <https://doi.org/10.1016/J.RENENE.2015.05.037>. Jan.
- [6] S. Ouédraogo, G.A. Faggiannelli, G. Pigelet, G. Notton, J.L. Duchaud, Performances of energy management strategies for a Photovoltaic/Battery microgrid considering battery degradation, *Sol. Energy* 230 (2021) 654–665, <https://doi.org/10.1016/J.SOLENER.2021.10.067>. Dec.
- [7] A.K. Azad, S. Parvin, Photovoltaic thermal (PV/T) performance analysis for different flow regimes: a comparative numerical study, *Int. J. Thermofluids* 18 (2023) 100319, <https://doi.org/10.1016/J.IJFT.2023.100319>. May.
- [8] A.H.A. Al-Waeli, K. Sopian, H.A. Kazem, M.T. Chaichan, Photovoltaic/Thermal (PV/T) systems: status and future prospects, *Renew. Sustain. Energy Rev.* 77 (2017) 109–130, <https://doi.org/10.1016/J.RSER.2017.03.126>.
- [9] A. Nahar, M. Hasanuzzaman, N.A. Rahim, Numerical and experimental investigation on the performance of a photovoltaic thermal collector with parallel plate flow channel under different operating conditions in Malaysia, *Sol. Energy* 144 (2017) 517–528, <https://doi.org/10.1016/J.SOLENER.2017.01.041>. Mar.
- [10] M.A. Yildirim, A. Cebula, M. Sutowicz, A cooling design for photovoltaic panels – water-based PV/T system, *Energy* 256 (2022) 124654, <https://doi.org/10.1016/J.ENERGY.2022.124654>. Oct.
- [11] M.R. Goma, M. Ahmed, H. Rezk, Temperature distribution modeling of PV and cooling water PV/T collectors through thin and thick cooling cross-fined channel box, *Energy Rep.* 8 (2022) 1144–1153, <https://doi.org/10.1016/J.EGYR.2021.11.061>. Apr.
- [12] A.H.A. Al-Waeli, K. Sopian, M.T. Chaichan, H.A. Kazem, H.A. Hasan, A.N. Al-Shamani, An experimental investigation of SiC nanofluid as a base-fluid for a photovoltaic thermal PV/T system, *Energy Convers. Manag.* 142 (2017) 547–558, <https://doi.org/10.1016/J.ENCONMAN.2017.03.076>. Jun.
- [13] S.R. Abdallah, H. Saidani-Scott, O.E. Abdellatif, Performance analysis for hybrid PV/T system using low concentration MWNT (water-based) nanofluid, *Sol. Energy* 181 (2019) 108–115, <https://doi.org/10.1016/J.SOLENER.2019.01.088>. Mar.
- [14] I. Karaaslan, T. Menlik, Numerical study of a photovoltaic thermal (PV/T) system using mono and hybrid nanofluid, *Sol. Energy* 224 (2021) 1260–1270, <https://doi.org/10.1016/J.SOLENER.2021.06.072>. Aug.
- [15] A.M. Elbreki, et al., The role of climatic-design-operational parameters on combined PV/T collector performance: a critical review, *Renew. Sustain. Energy Rev.* 57 (2016) 602–647, <https://doi.org/10.1016/J.RSER.2015.11.077>. May.
- [16] A.N. Al-Shamani, K. Sopian, S. Mat, H.A. Hasan, A.M. Abed, M.H. Ruslan, Experimental studies of rectangular tube absorber photovoltaic thermal collector with various types of nanofluids under the tropical climate conditions, *Energy Convers. Manag.* 124 (2016) 528–542, <https://doi.org/10.1016/J.ENCONMAN.2016.07.052>. Sep.
- [17] H. Fayaz, R. Nasrin, N.A. Rahim, M. Hasanuzzaman, Energy and exergy analysis of the PVT system: effect of nanofluid flow rate, *Sol. Energy* 169 (2018) 217–230, <https://doi.org/10.1016/J.SOLENER.2018.05.004>. Jul.
- [18] T.K. Murtadha, A.A. Hussein, Optimization the performance of photovoltaic panels using aluminum-oxide nanofluid as cooling fluid at different concentrations and one-pass flow system, *Results Eng* 15 (2022) 100541, <https://doi.org/10.1016/J.RINENG.2022.100541>. Sep.

- [19] S. Diwania, R. Kumar, S.K. Singh, G.S. Dua, P. Khetrapal, Performance assessment of a serpentine tube PVT system using Cu and TiO₂ nanofluids: an experimental study, *J. Brazilian Soc. Mech. Sci. Eng.* 44 (2) (2022) 1–18, <https://doi.org/10.1007/S40430-022-03366-5/FIGURES/19>, Feb.
- [20] S. Diwania, M. Kumar, R. Kumar, A. Kumar, V. Gupta, P. Khetrapal, Machine learning-based thermo-electrical performance improvement of nanofluid-cooled photovoltaic-thermal system (2022), <https://doi.org/10.1177/0958305X221146947>, Dec.
- [21] F.L.J. Diniz, C.V.P. Vital, L.A. Gómez-Malagón, Parametric analysis of energy and exergy efficiencies of a hybrid PV/T system containing metallic nanofluids, *Renew. Energy* 186 (2022) 51–65, <https://doi.org/10.1016/J.RENENE.2021.12.151>, Mar.
- [22] F. Hossain, M.R. Karim, A.A. Bhuiyan, A review on recent advancements of the usage of nano fluid in hybrid photovoltaic/thermal (PV/T) solar systems, *Renew. Energy* 188 (2022) 114–131, <https://doi.org/10.1016/J.RENENE.2022.01.116>, Apr.
- [23] H. Adun, M. Adedeji, M. Dagbasi, A. Babatunde, Amelioration of thermodynamic performance and environmental analysis of an integrated solar power generation system with storage capacities using optimized ternary hybrid nanofluids, *J. Energy Storage* 51 (2022) 104531, <https://doi.org/10.1016/J.EST.2022.104531>, Jul.
- [24] H. Adun, M. Adedeji, M. Dagbasi, O. Bamisile, M. Senol, R. Kumar, A numerical and exergy analysis of the effect of ternary nanofluid on performance of Photovoltaic thermal collector, *J. Therm. Anal. Calorim.* 145 (3) (2021) 1413–1429, <https://doi.org/10.1007/S10973-021-10575-Y/TABLES/6>, Aug.
- [25] H. Adun, M. Adedeji, T. Ruwa, M. Senol, D. Kavaz, M. Dagbasi, Energy, exergy, economic, environmental (4E) approach to assessing the performance of a photovoltaic-thermal system using a novel ternary nanofluid, *Sustain. Energy Technol. Assessments* 50 (2022) 101804, <https://doi.org/10.1016/J.SETA.2021.101804>, Mar.
- [26] A. Kazemian, A. Salari, T. Ma, H. Lu, Application of hybrid nanofluids in a novel combined photovoltaic/thermal and solar collector system, *Sol. Energy* 239 (2022) 102–116, <https://doi.org/10.1016/J.SOLENER.2022.04.016>, Jun.
- [27] A. Nahar, M. Hasanuzzaman, N.A. Rahim, S. Parvin, Numerical investigation on the effect of different parameters in enhancing heat transfer performance of photovoltaic thermal systems, *Renew. Energy* 132 (2019) 284–295, <https://doi.org/10.1016/J.RENENE.2018.08.008>, Mar.
- [28] X. Li, et al., Heat transfer enhancement of nanofluids with non-spherical nanoparticles: a review, *Appl. Sci.* 12 (2022) 4767, <https://doi.org/10.3390/APPL12094767>, 12, no. 9, p. 4767, May 2022.
- [29] M.M. Rienecker, et al., MERRA: NASA's modern-era retrospective analysis for research and applications, *J. Clim.* 24 (14) (2011) 3624–3648, <https://doi.org/10.1175/JCLI-D-11-00015.1>, Jul.
- [30] R. Müller, U. Pfeifroth, C. Träger-Chatterjee, J. Trentmann, R. Cremer, Digging the METEOSAT treasure—3 decades of solar surface radiation, 2015, Vol. 7, Pages 8067–8101, *Remote Sens* 7 (6) (2015) 8067–8101, <https://doi.org/10.3390/RS70608067>, Jun.
- [31] I. Staffell, S. Pfenniger, Using bias-corrected reanalysis to simulate current and future wind power output, *Energy* 114 (2016) 1224–1239, <https://doi.org/10.1016/J.ENERGY.2016.08.068>, Nov.
- [32] M.M. Rahman, H.F. Öztöp, M. Steele, A.G. Naim, K. Al-Salem, T.A. Ibrahim, Unsteady natural convection and statistical analysis in a CNT–water filled cavity with non-isothermal heating, *Int. Commun. Heat Mass Transf.* 64 (2015) 50–60, <https://doi.org/10.1016/J.ICHEATMASSTRANSFER.2015.02.012>, May.
- [33] A.K. Azad, M.M. Shuvo, R.H. Kabir, K.M. Rabbi, M.F. Karim, M.M. Rahman, Heat transfer augmentation in a diamond shaped enclosure utilizing CNT-water Nanofluid, *Int. Commun. Heat Mass Transf.* 116 (2020) 104647, <https://doi.org/10.1016/J.ICHEATMASSTRANSFER.2020.104647>, Jul.
- [34] Y. Khanjari, A.B. Kasaeian, F. Pourfayaz, Evaluating the environmental parameters affecting the performance of photovoltaic thermal system using nanofluid, *Appl. Therm. Eng.* 115 (2017) 178–187, <https://doi.org/10.1016/J.APPLTHERMALENG.2016.12.104>, Mar.
- [35] A. Kazemian, A. Salari, A. Hakkaki-Fard, T. Ma, Numerical investigation and parametric analysis of a photovoltaic thermal system integrated with phase change material, *Appl. Energy* 238 (2019) 734–746, <https://doi.org/10.1016/J.APENENERGY.2019.01.103>, Mar.
- [36] A. Nahar, *Numerical Investigation and Modelling of Solar Photovoltaic/Thermal Systems*, 2017, pp. 1982–2004. *Thesis*.
- [37] A.S. Joshi, A. Tiwari, G.N. Tiwari, I. Dincer, B.V. Reddy, Performance evaluation of a hybrid photovoltaic thermal (PV/T) (glass-to-glass) system, *Int. J. Therm. Sci.* 48 (1) (2009) 154–164, <https://doi.org/10.1016/J.IJTHERMALSCI.2008.05.001>, Jan.
- [38] M. Farbod, A. Ahangarpour, S.G. Etemad, Stability and thermal conductivity of water-based carbon nanotube nanofluids, *Particuology* 22 (2015) 59–65, <https://doi.org/10.1016/J.PARTIC.2014.07.005>, Oct.
- [39] S. Sreekumar, N. Shah, J.D. Mondol, N. Hewitt, S. Chakrabarti, Numerical investigation and feasibility study on MXene/water nanofluid based photovoltaic/thermal system, *Clean. Energy Syst.* 2 (2022) 100010, <https://doi.org/10.1016/J.CLES.2022.100010>, Jul.
- [40] R. Hossain, M.J. Hasan, A.K. Azad, M.M. Rahman, Numerical study of low Reynolds number effect on MHD mixed convection using CNT-oil nanofluid with radiation, *Results Eng* 14 (2022) 100446, <https://doi.org/10.1016/J.RINENG.2022.100446>, Jun.
- [41] M. Hemmat Esfe, S. Saedodin, O. Mahian, S. Wongwises, Thermophysical properties, heat transfer and pressure drop of COOH-functionalized multi walled carbon nanotubes/water nanofluids, *Int. Commun. Heat Mass Transf.* 58 (2014) 176–183, <https://doi.org/10.1016/J.ICHEATMASSTRANSFER.2014.08.037>, Nov.
- [42] E. Gutierrez-Miravete, B. Fontenault, Modeling a combined photovoltaic-thermal panel, *Proceedings of the 2012 COMSOL Conference, Milan, Italy* 10 (2012) [Online]. Available: <https://www.comsol.com/paper/modeling-a-combined-photovoltaic-thermal-panel-13004>. (Accessed 9 November 2022).